



Catalytic gasification of indole in supercritical water



Yang Guo^{a,b}, Shuzhong Wang^a, Thomas Yeh^b, Phillip E. Savage^{b,c,*}

^a Key Laboratory of Thermo-Fluid Science and Engineering, Ministry of Education, School of Energy and Power Engineering, Xi'an Jiaotong University, Xi'an, Shaanxi 710049, P.R. China

^b Department of Chemical Engineering, University of Michigan, 2300 Hayward St., Ann Arbor, MI 48109-2136, USA

^c Department of Chemical Engineering, Pennsylvania State University, University Park, PA 16802, USA

ARTICLE INFO

Article history:

Received 18 September 2014

Received in revised form

13 November 2014

Accepted 15 November 2014

Available online 21 November 2014

Keywords:

Supercritical water gasification

Bimetallic catalyst, Nickel

Ruthenium

Cerium oxide.

ABSTRACT

We tested Ru/C, Pt/C, Pd/C, Pt/Al₂O₃, Pd/Al₂O₃, activated carbon, and Ni–Ru/CeO₂ catalysts for the gasification of indole in supercritical water. All of the materials enhanced the gasification of this nitrogen-containing compound, but the bimetallic catalyst, Ni–Ru/CeO₂, showed the highest activity for producing CO and CH₄ and for converting indole. We focused on this catalyst in more detail. The catalyst loading in the reactor has no effect on the H₂ yield, but both CH₄ and CO₂ yields decrease with decreased loading. Water density has no statistically significant effect on the yield of gas products, but operating above the critical pressure of water is a prerequisite for the Ni–Ru composite catalyst to reach a high conversion of indole. The catalyst surface area and pore volume decrease from 5.91 m² g^{−1} and 0.0169 cm³ g^{−1} to 2.86 m² g^{−1} and 0.0137 cm³ g^{−1}, respectively, after an SCWG reaction time of 180 min. NiO species were detected in both fresh and used catalysts and may be due to oxidation of the reduced Ni metal during sample preparation for XPS analysis, and/or a strong interaction between metal and support possibly leading to the formation of cationic Ni species. These results point to potential benefits of using this bimetallic catalyst for SCWG of streams with recalcitrant N-containing compounds.

© 2014 Elsevier B.V. All rights reserved.

1. Introduction

Gasification of organic materials in supercritical water is a means of producing fuel gases (e.g., H₂, CH₄) from biomass, sludges, organic-laden wastewaters, and other organic materials with a high moisture content [1]. This technology is being considered for use with protein-containing materials such as algal biomass and with byproduct streams from proposed algal biorefineries [2–4]. For example, an algal biorefinery that uses hydrothermal carbonization as a pretreatment step for wet algal biomass prior to lipid extraction will produce lipid-extracted char as a solid byproduct. Converting the organic carbon in lipid-extracted char to fuel gases would provide energy for the biorefinery. Additionally, both hydrothermal carbonization and hydrothermal liquefaction of wet algal biomass will generate aqueous byproduct streams that are rich in organic compounds. Converting the organic carbon in the aqueous byproduct stream to fuel gases would provide energy for the biorefinery. Well over half of these aqueous-phase organic compounds contain nitrogen atoms, and lipid-extracted char is also rich in nitrogen [5]. There has been tremendous research effort on

understanding the gasification of materials and pure compounds that contain C, H, and O atoms, the principal constituents of terrestrial biomass, but far less on compounds that contain N atoms, which are abundant in microalgae and in algal biorefinery process streams [1,6,7].

Indole is a heterocyclic N-containing compound that is a product from hydrothermal treatment of algae. It is slow to gasify when using thermal energy and supercritical water alone [8]. The need to gasify N-containing compounds such as indole and the recalcitrance of such compounds suggest the use of catalysts to accelerate supercritical water gasification (SCWG). We are aware of only three previous studies on catalytic SCWG of N-containing model compounds. Chakinala et al. [9] and Kruse et al. [10] studied the catalytic effect of K₂CO₃/KHCO₃ on carbohydrate-amino acids mixtures. DiLeo et al. [11] examined glycine gasification over a Ni wire catalyst. Each of these studies showed that a catalyst can accelerate the gasification rate, but none of these studies used a conventional supported metal catalyst. The need to gasify effectively N-containing compounds in algal biorefinery streams, the recalcitrance of indole to uncatalyzed SCWG, and the absence of work on catalytic SCWG of N-containing compounds with supported metal catalysts motivated the work reported herein. We have examined a suite of potential SCWG catalysts and then explored and characterized the most effective catalyst in more detail.

* Corresponding author. Tel.: +1 814 867 5876; fax: +1 814 865 7846.

E-mail addresses: psavage@engr.psu.edu, psavage@umich.edu (P.E. Savage).

We used the literature on catalytic SCWG as a guide when selecting the catalysts for this study. Ni, Ru, Pt, and Pd are all active for SCWG, and Al_2O_3 and C are the supports most commonly used [12–20]. Therefore, we selected catalysts that used different combinations of these metals and supports. Additionally, the literature shows that Ni catalysts lose activity over time [12,14,15]. Waldner et al. [15] noted that Ni-catalyzed gasification in supercritical water achieved complete gasification, but after 50 h of continuous use, coke deactivated the catalyst. High catalytic activity for Ni was reported for SCWG of real biomass, but deactivation was also observed due to adsorption of intermediate products on the catalyst. [21] Elliott et al. [22] demonstrated that adding Cu, Ag, Sn, and Ru to a Ni catalyst can improve activity and prolong its life. Additionally, Zhang et al. [23,24] studied Ni–Ru/ γ - Al_2O_3 in SCWG and found that doping with Ru can improve the dispersion and stability. This prior work led us to include Ni–Ru catalysts in the present study.

In addition to using Al_2O_3 and C as catalyst supports, we employed CeO_2 . CeO_2 -supported noble metal catalysts show a high selective oxidation activity for CO, particularly for the water–gas shift reaction [25–29]. CeO_2 can also improve the dispersion and stability of the active metal [30]. Although much research has been devoted to CeO_2 -supported metal catalysts in relatively low-temperature hydrothermal reactions [28,29,31–33], little attention has been paid to it at SCWG conditions.

In this article, we screen different catalysts and then focus on the most effective (Ni–Ru/ CeO_2) for the SCWG of indole. We report on the influence of the Ni/Ru ratio, the catalyst loading, temperature, batch holding time, and water density.

2. Experimental

2.1. Materials

Activated carbon, Ru/C, Pt/C, Pd/C, Pt/ Al_2O_3 , Pd/ Al_2O_3 , and the solvents used in this investigation were purchased from Sigma-Aldrich and Fisher Scientific in high purity. The metal loading was 5 wt% in all of the purchased catalysts. The chemicals used for catalyst synthesis (CeO_2 , RuCl_3 , and $\text{Ni}(\text{NO}_3)_2 \cdot 6(\text{H}_2\text{O})$), were purchased from Strem and Sigma-Aldrich in high purity. We used 316 stainless-steel mini batch reactors constructed from a 1/2 in. Swagelok port connector, a cap, a 1/2 to 1/8 in. reducing union, a 9 in. length of 1/8 o.d. tubing, and a high-pressure valve. Prior to use in reactions, the assembled reactors were loaded with 2 mL of deionized water and heated to 500 °C for 60 min to expose the reactor walls to the hydrothermal reaction condition.

2.2. Catalyst preparation

The Ni–Ru bimetallic catalysts were prepared in-house. $\text{Ni}(\text{NO}_3)_2 \cdot 6(\text{H}_2\text{O})$, RuCl_3 , and deionized water were well mixed in the amounts needed for the desired Ni/Ru ratio and metal weight loading and allowed to sit for 6 h. One gram of CeO_2 was immersed in the solution and stirred for 12 h or overnight. The catalyst was fully dried at 120 °C and then ground using a mortar and pestle. The powder was collected in a quartz boat and then calcined in a Barnstead Thermolyne 21100 isothermal tube furnace in air. The temperature first increased 3 °C/min to 550 °C and that temperature was held for 240 min before switching off the furnace and allowing the catalyst to cool to room temperature. After calcination, the catalyst was reduced in flowing H_2 at 400 °C with the heating ramp and cooling identical to those used for calcination. We express the catalyst composition as “x wt%Ni–yRu/ CeO_2 ”, where x represents the weight percentage of active metal (Ni + Ru) in the catalyst and y is the mass ratio of Ru/Ni.

2.3. Experimental procedure

All SCWG experiments were done at 500 °C and an initial indole concentration of 0.3 mol/L. Unless otherwise specified, the batch holding time, catalyst loading relative to indole mass, and water density were 30 min, 25 wt% and 0.115 g/mL, respectively.

After loading the catalyst, water, and indole into each reactor in the desired amounts, we sealed the reactors and connected them to a vacuum pump. Air was removed from the reactor under a vacuum of 1.5 psi. Then the reactors were pressurized to 50 psi by helium, which served as an internal standard for gas product analysis. At the same time, the gas tightness of the reactors was tested by immersing them into water.

The reaction time began when we placed the reactors into a Techne fluidized sand bath preheated to the reaction temperature. The reactors reached the set point temperature within approximately 2 min. The reactors were constantly agitated by a wrist action shaker. After the desired reaction time had elapsed, we removed the reactors from the sand bath and immersed them into a room-temperature water bath where they remained for at least 40 min to quench the reaction.

2.4. Analytical chemistry

Gas analysis was performed by using an Agilent 6890N gas chromatograph equipped with a thermal conductivity detector (TCD) and a Supelco 60/80 mesh Carboxen 1000 packed column (15 ft \times 1/8 in. O.D.). The chromatographic procedure has been reported previously [8].

After gas product analysis, we analyzed liquid products. The reactors were opened carefully and we rinsed all internal surfaces at least five times using acetone. Enough acetone was added to result in a final volume of 10 mL. The solution and catalyst particles were transferred to a centrifuge tube which was centrifuged at 4000 rpm for 20 min. Qualitative analyses of liquid samples occurred on an Agilent 6890N gas chromatograph and 5793N mass spectrometer (GC–MS) equipped with a HP-5MS capillary column (50 m \times 0.20 mm I.D., 0.33 μm film thickness) and using helium as the carrier gas. Another Agilent 6890 GC equipped with an HP-5 column and a flame ionization detector (GC–FID) was used for quantitative analysis. The amount of each compound in the sample was obtained by using linear calibrations prepared using standards. Most experiments were replicated at least three times, and we report mean values and the standard deviation about the mean as the measure of uncertainty.

A Kratos AXIS Ultra DLD X-ray photoelectron spectrometer (XPS) determined the oxidation states of Ru and Ni in the catalyst samples. We prepared the samples by adhering the powdered catalysts to a copper tape. We determined the appropriate energy windows by performing a full scan of the available energies. Then the narrower energy windows were used to take more detailed scans for determining the characteristic binding energies. The energy values obtained were corrected according to the carbon 1s binding energy.

The surface area of each catalyst sample was determined using a Micromeritics ASAP 2010 surface area analyzer, which performed N_2 physisorption. Before analysis, the samples were loaded into a quartz tube, heated to 350 °C under vacuum for 2 h, and subsequently backfilled with He and weighed to obtain the sample mass.

Transmission electron microscopy (TEM) was performed with a JEOL 2010F instrument equipped with HAADF (high angle annular dark field) and an energy-dispersive X-ray detector at an accelerating voltage of 200 kV. TEM samples were prepared by creating a suspension of the catalyst particles in ethanol. Five drops of the catalyst suspension were dropped onto a copper grid with holey carbon, and the excess solvent was removed.

3. Results and discussion

3.1. Catalyst screening

Figs. 1 and 2 compare gas yields and liquid product concentrations over the different catalysts examined. Benzene, toluene, and aniline were quantitatively analyzed because they are the most abundant products. Fig. 1 confirms that indole is difficult to gasify without adding catalyst. The gas yield from the experiment without catalyst was the lowest for all runs and the yields of CO, CH₄, and C₂H₆ were nearly zero. Pt and Pd provide essentially the same gas yields regardless of whether supported on C or Al₂O₃, and Pt always gasified more of the carbon than did Pd. Activated carbon exhibits some catalytic activity for indole SCWG, but the gas yields are much lower than when a metal is also present on this support. The indole conversion and the gas yields are the highest with the Ni–Ru/CeO₂ catalyst and the Ru/C catalyst. The production of carbon-rich gases can likely be attributed to Ru enhancing C–C bond cleavage [19]. For these two catalysts, the yield of aniline exceeded the yields of toluene and benzene combined. It seems that the Ru-containing catalysts are more active for formation of aniline, which could lead to the accumulation of aniline and its derivatives during the hydrothermal treatment. It appears that the use of different catalysts provides opportunities to alter product selectivities and hence rates of different pathways.

Though the hydrogen yield from 30 wt% Ni–0.1Ru/CeO₂ is the highest among the supported metal catalysts, it is much lower than those reported by Zhang et al. [34] for SCWG of glucose (1.8–9.7 mol H₂/mol glucose) over a similar catalyst, because glucose is easier to gasify. Another difference with this previous study is the relatively high yield of CH₄ observed in this experiment, whereas Zhang et al. [34] found that a Ni–Ru catalyst significantly reduced CH₄ formation relative to that from a control experiment without catalyst.

We calculated the carbon and hydrogen gasification efficiencies as the number of C or H atoms in the gas products divided by the number of C or H atoms in the indole loaded into the reactor. The gasification efficiency (GE) measures the portion of the feed material that was converted into gaseous products. We also calculated the selectivity for carbon and hydrogen as the number of C or H atoms in the gas products divided by the number of C or H atoms in the indole that had reacted. A selectivity of 100% would indicate that all of the C or H atoms in the indole that had reacted were converted into gaseous products. A selectivity of less than 100% indicates that some of the reacted indole formed intermediate liquid-phase products.

Table 1 shows the results of these calculations for the different catalysts. We first note that both gasification efficiencies and both selectivities have their highest values for the Ni–Ru catalyst. This bimetallic catalyst is superior to the others tested for SCWG of indole. Ru/C, a well-established SCWG catalyst, was the next most effective material. We next note that regardless of the catalyst, the carbon gasification efficiency (CGE) always exceeded the hydrogen gasification efficiency (HGE). The hydrogen atoms in indole are more difficult to transfer into gaseous products than are the carbon atoms. The selectivity for hydrogen exceeds 100% for the Ni–Ru catalyst. This result indicates that hydrogen atoms derived from water molecules appear in the products formed during gasification.

3.2. Influence of Ru/Ni ratio

The Ni–Ru/CeO₂ catalyst provided the highest yields of H₂ and CH₄, the highest indole conversion, the highest H and C gasification efficiencies, and the highest gas-phase selectivities for C and H. Therefore, we examined the Ni–Ru binary catalyst in more detail. In this section, we report on the influence of the Ru/Ni ratio in the catalyst by examining Ru and Ni on CeO₂ in four different ratios (30 wt% Ni, 30 wt% Ni–0.1Ru, 30 wt% Ni–0.5Ru and 5 wt% Ru).

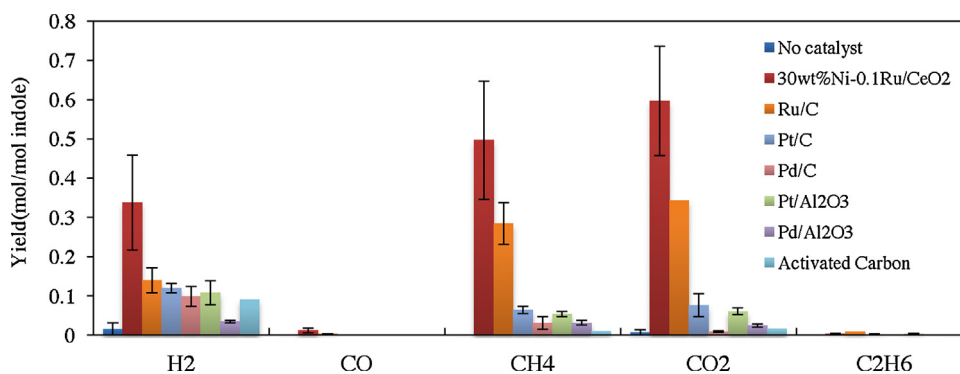


Fig. 1. Gas product yield over different catalysts.

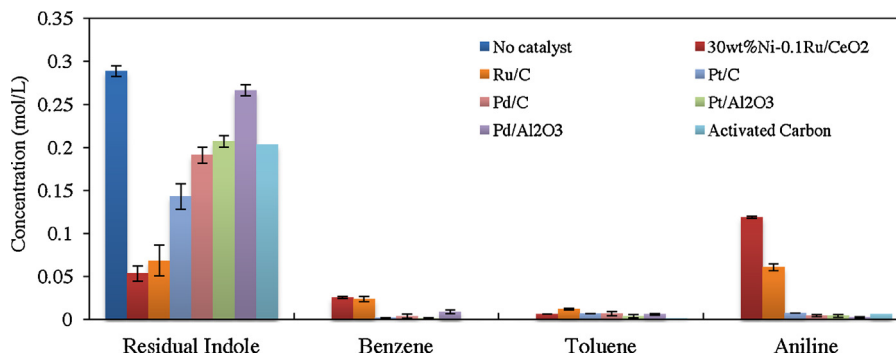


Fig. 2. Liquid product concentrations over different catalysts.

Table 1
Gasification efficiencies and selectivities for different catalysts.

Catalyst	CGE ^a (%)	HGE ^b (%)	C selectivity (%)	H selectivity (%)
None	0.10 ± 0.09	0	0.10 ± 0.09	0.49 ± 0.45
30 wt%Ni–0.1Ru/CeO ₂	13.9 ± 3.7	0.38 ± 0.12	75 ± 16	202 ± 60
Ru/C	8.1 ± 1.6	0.21 ± 0.04	36.8 ± 10.2	95 ± 24
Pt/C	1.84 ± 0.46	0.07	3.9 ± 1.4	15.6 ± 1.9
Pd/C	0.51 ± 0.18	0.05	0.79 ± 0.24	7.25 ± 0.03
Pt/Al ₂ O ₃	1.54 ± 0.22	0.07	2.23 ± 0.24	9.49 ± 0.89
Pd/Al ₂ O ₃	0.71 ± 0.12	0.03	0.80 ± 0.16	3.20 ± 0.53
Activated carbon	0.37	0.03	0.54	4.84

^a Carbon gasification efficiency.

^b Hydrogen gasification efficiency.

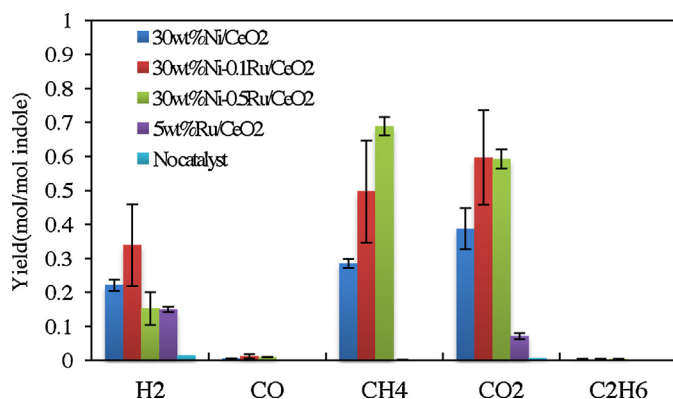


Fig. 3. Gas yields over Ni–Ru/CeO₂ at different Ru/Ni ratios.

Figs. 3 and 4 compare the gas yields and liquid product concentrations obtained from SCWG over catalysts with different Ru/Ni ratios. Though 5 wt% Ru/C was an effective SCWG catalyst, as shown in Figs. 1 and 2, changing the support to CeO₂ reduced the activity. The surface area of the CeO₂ support (BET analysis results are presented in a later section) being much lower than that of the activated carbon support may be responsible for this difference. Nevertheless, all the catalysts in view in this section are on the same support, which enables a comparison of the effects of the different pure metals and binary composition. The two Ru–Ni catalysts considered gave the highest indole conversions and the highest methane yields. Though the mean methane yield is higher for the 0.5Ru catalyst, the uncertainty in the data prevent one from concluding that this difference is statistically significant. Over monometallic Ni, toluene is the most abundant liquid-phase product, whereas aniline was the most abundant product over the binary catalysts. The data in Figs. 3 and 4 show that the Ni–Ru bimetallic

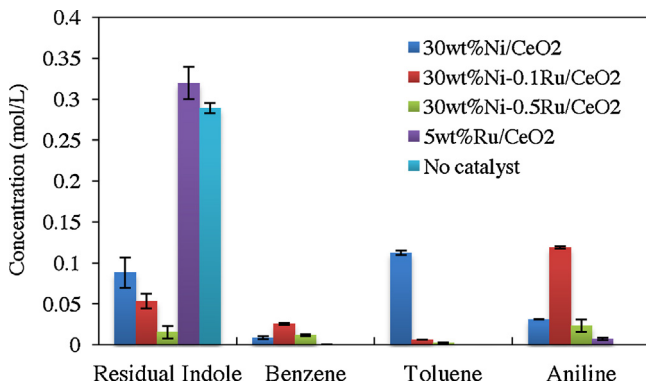


Fig. 4. Concentration of main liquid products over Ni–Ru/CeO₂ at different Ru/Ni ratios.

catalyst provided higher indole conversions and higher gas yields than did either Ni or Ru alone.

3.3. Influence of catalyst loading

We examined the influence of catalyst loading (25.1, 15.8, 7.2, and 3.8 wt%) at 500 °C. A 30 wt% Ni–0.1Ru/CeO₂ catalyst was used in all runs. Fig. 5 shows no effect of loading on the H₂ yield, but both the CH₄ and CO₂ yields decrease with decreased catalyst loading. The average rates of methane production at each loading are 0.47 ± 0.14, 0.45 ± 0.15, 0.44 ± 0.24, and 0.21 ± 0.05 mol CH₄ min^{−1} gcat^{−1}. With the exception of the lowest loading, these average rates are all about the same, which one would expect for a reaction first-order in catalyst.

Fig. 6 shows that the concentration of residual indole increases with decreased catalyst loading. The largest increase occurred when the catalyst loading decreased from 25.1 to 15.8 wt%. The concentrations of benzene, toluene, and aniline decreased as the catalyst loading decreased. The highest aniline concentration in the liquid products was 0.12 M at the highest catalyst loading. The average rates of aniline production at each loading are 0.11, 0.08 ± 0.01, 0.11 ± 0.03, and 0.11 ± 0.02 mol min^{−1} gcat^{−1}. These rates being similar suggest that the reaction is first order in catalyst, as one would expect.

3.4. Influence of water density

Figs. 7 and 8 show gas yields and liquid product concentrations from indole SCWG at different water densities, 500 °C, and with an average loading of 25 wt% of the 30 wt%Ni–0.1Ru/CeO₂ catalyst. Fig. 7 shows that water density has no statistically significant effect on gas products. Fig. 8 shows that the residual indole concentration at a water density of 0.068 g/mL is much higher than that obtained at the other three water densities, and the concentrations of benzene, toluene, and aniline are the lowest. Otherwise, the water density has no effect on the concentrations of the liquid-phase products. Based on the properties of pure water, a water density of 0.068 g/mL at 500 °C corresponds to a reactor pressure

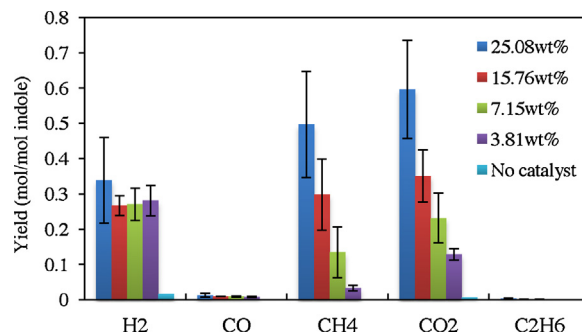


Fig. 5. Gas product yields at different catalyst loadings (wt% relative to indole).

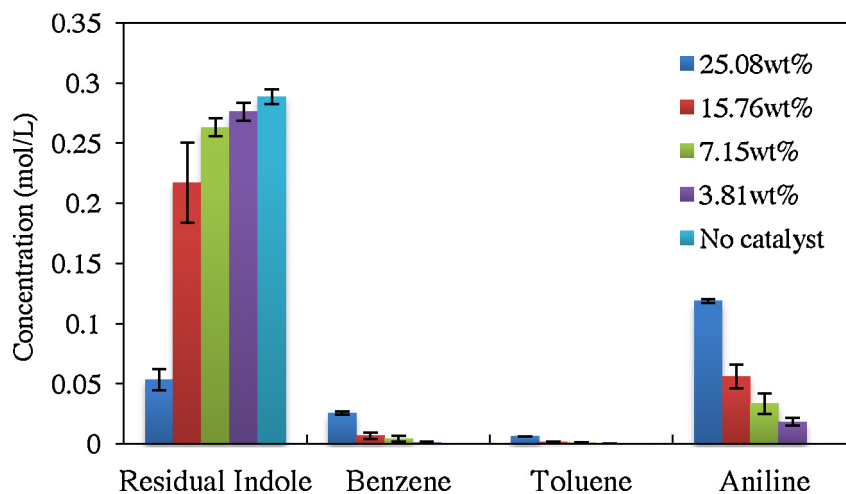


Fig. 6. Liquid product concentrations at different catalyst loadings (wt% relative to indole).

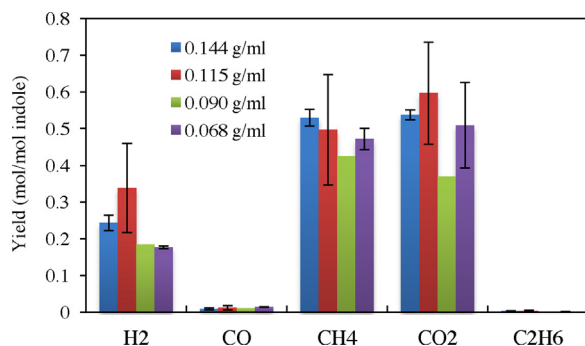


Fig. 7. Gas product yields at different water densities.

of 20 MPa at reaction conditions, which is below the critical pressure of water. It seems that a supercritical pressure is required to achieve the high conversions.

3.5. Identifying liquid-phase products

This section provides information about the liquid products formed during catalytic SCWG of indole. Fig. 9 shows the total ion chromatogram of the liquid product samples collected from a catalytic reaction of indole in SCW at 500 °C for 30 min over 30 wt%Ni–0.5Ru/CeO₂ and 30 wt%Ni–0.1Ru/CeO₂. Table 2 provides the identification of each numbered peak in Fig. 9. Compounds for which the identification is tentative, either because an authentic standard was not commercially available or due to poor match quality between the sample mass spectrum and the MS library, are

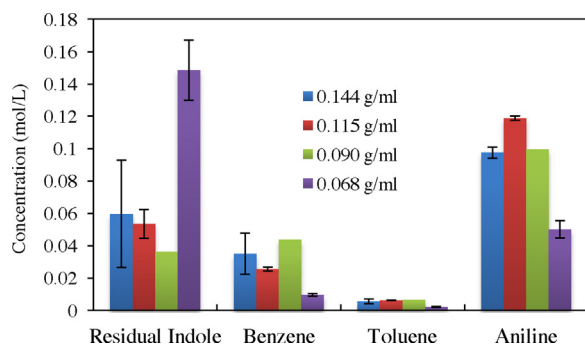


Fig. 8. Liquid product concentrations at different water densities.

indicated by including the GC–MS match quality in parentheses. The higher the match quality (100 is a perfect match), the more likely is the tentative identification to be correct.

The main products include benzene, toluene, aniline derivatives, diamines, tetrahydropyrroles, pyrimidines, indole, and methylin-dole. The selectivity for these compounds changes with the Ru/Ni ratio. The higher Ru/Ni ratio produced more of the compound tentatively identified as a tetrahydropyrrole derivative (peak 6), but less aniline (peak 4), 2-methyl-benzenamine (peak 7), and 7-methyl-6,7-dihydro-5H-1-pyridine (peak 8). This difference indicates that selectivity for aniline is higher at the lower Ru/Ni ratio. C–C bond breaking is enhanced with increasing Ru content, but C–N bond breaking is not facilitated over Ru-containing catalysts, which results in a number of nitrogen-containing intermediates appearing in the liquid product.

3.6. Catalyst characterization

This section presents information about the surface and bulk structure and composition of the catalyst. These results help to relate the macroscopic/microscopic properties of the material with its catalytic properties.

Fig. 10 shows the transmission electron microscope (TEM) (Fig. 10a) and scanning TEM (Fig. 10b–d) images of a 30 wt%Ni–0.1Ru/CeO₂ catalyst prepared by calcination at 550 °C and reduction in H₂ at 400 °C. Fig. 10a shows the presence of many Ni–Ru metal particles (dark spots) with diameter <2 nm on the CeO₂ support. Fig. 10 also provides elemental distribution results from energy-dispersive X-ray spectroscopy (EDS) analysis. The light area in the EDS scan (Fig. 10b) is the region with a dense metal distribution. The green and yellow points on the black background of Fig. 10c and d represent the positions of Ru and Ni atoms, respectively. In general, the Ru atoms are evenly distributed amongst the Ni atoms, and Ni is more abundant, as expected based on the ratio of metals used in the catalyst synthesis.

Catalyst properties such as pore structure, surface area, and pore volume can influence the catalytic activity. Table 3, which compares these properties for the fresh and used catalyst, shows that the surface area and pore volume decrease from 5.91 m² g^{−1} and 0.0169 cm³ g^{−1}, respectively, to 2.86 m² g^{−1} and 0.0137 cm³ g^{−1} after a reaction time of 180 min. The average pore radius, however, increases from 53.8 to 305 Å. It is not clear whether this change in surface morphology has adverse effects on the catalyst life, which still needs to be comprehensively evaluated in a continuous flow reactor system.

Table 2
Identities and relative amounts of compounds in Fig. 9.

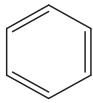
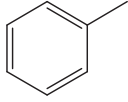
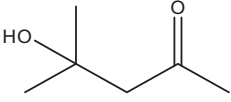
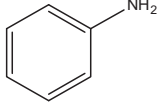
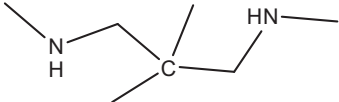
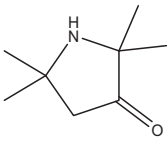
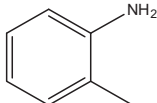
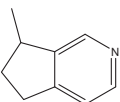
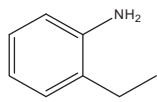
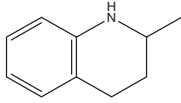
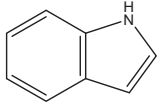
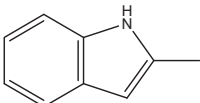
Peak no.	RT (min)	Name (and match quality)	Structure
1	8.353	Benzene	 .eps
2	12.257	Toluene	 .eps
3	15.303	2-Pentanone, 4-hydroxy-4-methyl- (78)	 .eps
4	20.957	Aniline	 .eps
5	21.613	2-Methyl- <i>N,N'</i> ,2,2-tetramethylpropane-1,3-diamine (33)	 .eps
6	21.989	2,2,5,5-Tetramethyl-3-oxo-2,3,4,5-tetrahydropyrrole (43)	 .eps
7	24.580	Benzenamine, 2-methyl-	 .eps
8	25.752	7-Methyl-6,7-dihydro-5 <i>H</i> -1-pyridine	 .eps
9	27.558	Benzenamine, 2-ethyl-	 .eps
10	27.816	Quinoline,1,2,3,4-tetrahydro-2-methyl-(72)	 .eps
11	32.146	Indole	 .eps
12	35.018	1 <i>H</i> -Indole, 2-methyl-	 .eps

Table 3
Physical properties of fresh and used 30 wt%Ni–0.5Ru/CeO₂ catalysts.

	BET surface area (m ² g ^{−1})	Pore volume (cm ³ g ^{−1})	Average pore radius (Å)
Fresh catalyst	5.91	0.0169	53.8
Used catalyst (500 °C, 180 min; 25 wt% catalyst loading)	2.86	0.0137	305

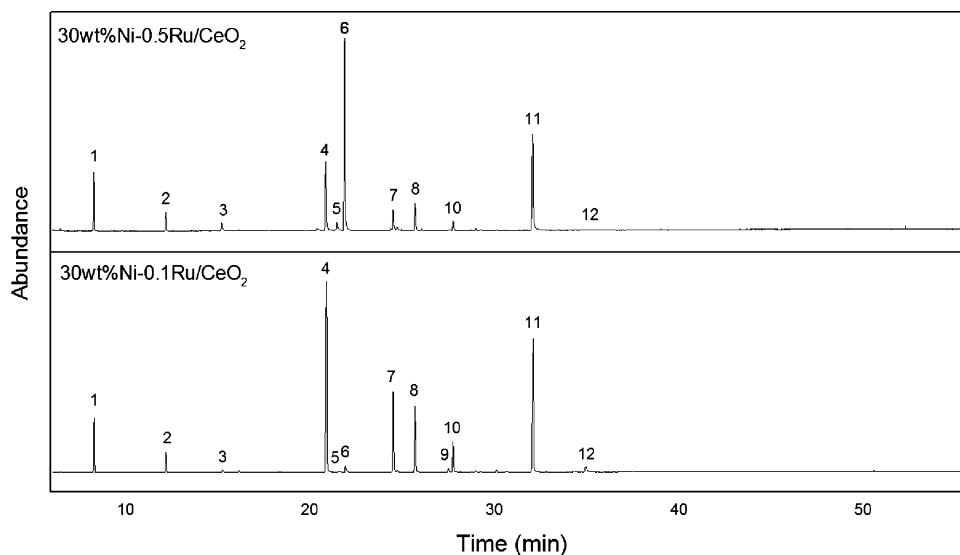


Fig. 9. Total ion chromatogram for the liquid samples from reactions of indole in SCW (500 °C, 300 bar, and 30 min) over catalysts with different Ru/Ni ratios.

X-ray photoelectron spectroscopy (XPS) analyses were carried out to explore the chemical composition of the surface layers of the Ni–Ru/CeO₂ catalyst and whether it differs before and after reaction. Fig. 11a, which presents the XPS spectra of Ni 2p, shows a peak at around 853 eV corresponding to metallic Ni. However, a satellite peak around 858 eV corresponding to NiO can also be observed in all samples. Since the NiO peak appears in both the fresh and used catalysts, it is not arising from the SCWG reaction. Two possibilities for

the formation of Ni²⁺ species are: (1) oxidation of reduced Ni metal by oxygen in air during sample preparation for XPS analysis; (2) a strong interaction between the metal and the oxide support possibly leading to the formation of cationic Ni species. The existence of metal–support interactions in CeO₂-supported metal catalysts has been established by many researchers [35–37]. CeO₂ is a redox catalyst support, so a strong interaction may exist between the Ni metal and the CeO₂, which would result in the oxidation of Ni to Ni²⁺.

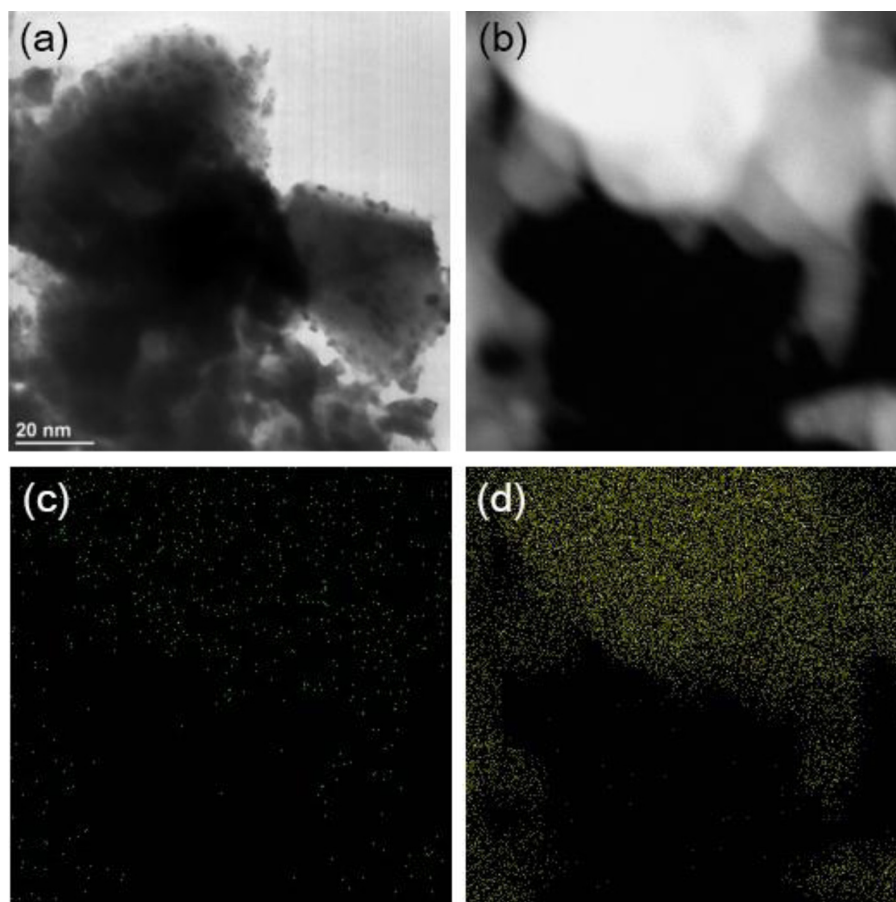


Fig. 10. TEM image and EDS analysis of Ni–Ru/CeO₂ catalyst: (a) TEM image; (b) EDS scan area; (c) Ru distribution; (d) Ni distribution.

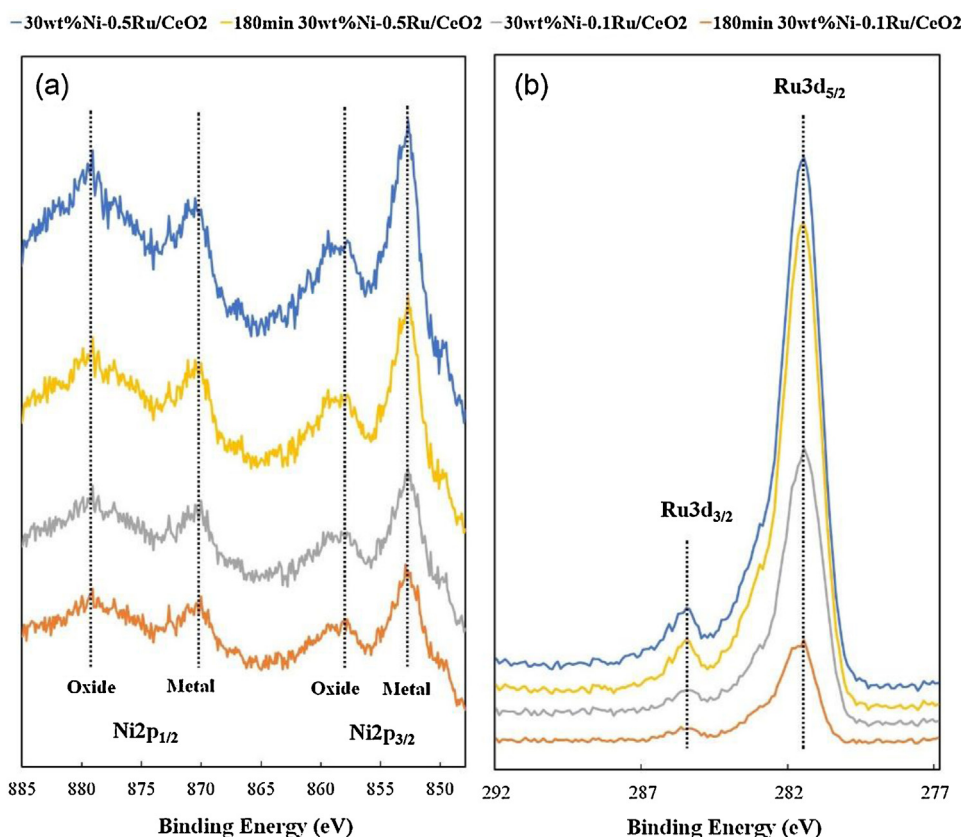


Fig. 11. Ni 2p and Ru 3d XPS spectra of fresh and used (after 180 min) 30 wt%Ni–0.5Ru/CeO₂ and 30 wt%Ni–0.1Ru/CeO₂.

Fig. 11b shows that the peaks for Ru appear at the same binding energies in the fresh and used catalysts and for both the 50% Ru and the 10% Ru catalysts. Overall, the XPS analysis of the fresh and used catalysts with two different Ru:Ni ratios showed no changes occurring as a result of exposure to the SCWG reaction conditions.

4. Conclusions

This first report on SCWG of a N-containing compound over supported metal catalysts shows that Pt, Pd, Ru, and Ni are all active for indole gasification. Bimetallic Ni–Ru/CeO₂ catalysts are even more active than any of the monometallic catalysts tested. The amount of this bimetallic catalyst loaded into the reactor had no effect on the H₂ yield, but both the CH₄ and CO₂ yields and the concentrations of benzene, toluene, and aniline increase with increased catalyst loading. The water density has no clear effect on the yields of the gas products, but a pressure above the critical pressure of water was required for the Ni–Ru composite catalyst to generate a high conversion of indole. The surface area and pore volume of the used catalyst are lower than in the fresh catalyst, but catalyst use at SCWG conditions induced no change in its surface composition. This work has identified a promising heterogeneous catalyst for SCWG of recalcitrant N-containing compounds that will be abundant in algal biorefinery process streams.

Acknowledgement

This research was supported by Postdoctoral Science Foundation of China (126540), Jiangsu Province Natural Science Foundation of China (BK20140406), National Natural Science Foundation of China (51406146), and Shaanxi Province Natural Science Foundation of China (2014JQ2081).

References

- [1] A. Kruse, *Biofuels, Bioproducts Biorefining* 2 (2008) 415–437.
- [2] P.E. Savage, *Science* 338 (2012) 1039–1040.
- [3] J. Akhtar, N.A.S. Amin, *Renew. Sustainable Energy Rev.* 15 (2011) 1615–1624.
- [4] D. López Barreiro, W. Prins, F. Ronsse, W. Brilman, *Biomass Bioenergy* 53 (2013) 113–127.
- [5] R.B. Levine, C.O.S. Sierra, R. Hockstad, W. Obeid, P.G. Hatcher, P.E. Savage, *Environ. Progr. Sustainable Energy* 32 (2013) 962–975.
- [6] C. Douglas, *Elliott Biofuels Bioprod. Biorefining* 2 (2008) 254–265.
- [7] P.E. Savage, *J. Supercrit. Fluids* 47 (2009) 407–414.
- [8] Y. Guo, S. Wang, C.M. Huelsman, P.E. Savage, *J. Supercrit. Fluids* 73 (2013) 161–170.
- [9] A.G. Chakinala, D.W.F. Brilman, W.P.M. van Swaaij, S.R.A. Kersten, *Ind. Eng. Chem. Res.* 49 (2009) 1113–1122.
- [10] A. Kruse, P. Maniam, F. Spieler, *Ind. Eng. Chem. Res.* 46 (2007) 87–96.
- [11] G.J. DiLeo, M.E. Neff, S. Kim, P.E. Savage, *Energy Fuels* 22 (2008) 871–877.
- [12] H. Nakagawa, A. Namba, M. Böhlmann, K. Miura, *Fuel* 83 (2004) 719–725.
- [13] G.J. DiLeo, M.E. Neff, P.E. Savage, *Energy Fuels* 21 (2007) 2340–2345.
- [14] D.C. Elliott, T.R. Hart, G.G. Neuenschwander, *Ind. Eng. Chem. Res.* 45 (2006) 3776–3781.
- [15] M.H. Waldner, F. Vogel, *Ind. Eng. Chem. Res.* 44 (2005) 4543–4551.
- [16] M. Osada, T. Sato, M. Watanabe, T. Adschiri, K. Arai, *Energy Fuels* 18 (2004) 327–333.
- [17] T. Sato, M. Osada, M. Watanabe, M. Shirai, K. Arai, *Ind. Eng. Chem. Res.* 42 (2003) 4277–4282.
- [18] X. Hao, L. Guo, X. Zhang, Y. Guan, *Chem. Eng. J.* 110 (2005) 57–65.
- [19] A.J. Byrd, K.K. Pant, R.B. Gupta, *Ind. Eng. Chem. Res.* 46 (2007) 3574–3579.
- [20] A.J. Byrd, K.K. Pant, R.B. Gupta, *Fuel* 87 (2008) 2956–2960.
- [21] T. Yoshida, Y. Oshima, Y. Matsumura, *Biomass Bioenergy* 26 (2004) 71–78.
- [22] D.C. Elliott, L.J. Sealock, E.G. Baker, *Ind. Eng. Chem. Res.* 32 (2002) 1542–1548.
- [23] L. Zhang, P. Champagne, C. Xu, *Int. J. Hydrogen Energy* 36 (2011) 9591–9601.
- [24] L. Zhang, C. Xu, P. Champagne, *Fuel* 96 (2012) 541–545.
- [25] H. Fajardo, L.D. Probst, N.V. Carreño, I.S. Garcia, A. Valentini, *Catal. Lett.* 119 (2007) 228–236.
- [26] T. Bunluesin, R.J. Gorte, G.W. Graham, *Appl. Catal. B Environ.* 15 (1998) 107–114.
- [27] X. Wang, R.J. Gorte, J.P. Wagner, *J. Catal.* 212 (2002) 225–230.
- [28] Q. Fu, A. Weber, M. Flytzani-Stephanopoulos, *Catal. Lett.* 77 (2001) 87–95.
- [29] Q. Fu, S. Kudriavtseva, H. Saltsburg, M. Flytzani-Stephanopoulos, *Chem. Eng. J.* 93 (2003) 41–53.
- [30] P. Bera, A. Gayen, M.S. Hegde, N.P. Lalla, L. Spadaro, F. Frusteri, F. Arena, *J. Phys. Chem. B* 107 (2003) 6122–6130.

- [31] Q. Fu, H. Saltsburg, M. Flytzani-Stephanopoulos, *Science* 301 (2003) 935–938.
- [32] Y. Li, Q. Fu, M. Flytzani-Stephanopoulos, *Appl. Catal. B Environ.* 27 (2000) 179–191.
- [33] N.A. Koryabkina, A.A. Phatak, W.F. Ruettinger, R.J. Farrauto, F.H. Ribeiro, J. Catal. 217 (2003) 233–239.
- [34] L.H. Zhang, P. Champagne, C.B. Xu, *Bioresour. Technol.* 102 (2011) 8279–8287.
- [35] C. Force, J.P. Belzunegui, J. Sanz, A. Martínez-Arias, J. Soria, J. Catal. 197 (2001) 192–199.
- [36] K. Sun, W. Lu, M. Wang, X. Xu, *Appl. Catal. A: Gen.* 268 (2004) 107–113.
- [37] J. Kugai, V. Subramani, C. Song, M.H. Engelhard, Y.-H. Chin, J. Catal. 238 (2006) 430–440.